

## ARTICLE OPEN



# Enhanced surface temperature over India during 1980–2020 and future projections: causal links of the drivers and trends

Rahul Kumar<sup>1</sup>, Jayanarayanan Kuttipurath<sup>1</sup>✉, G. S. Gopikrishnan<sup>1</sup>, Pankaj Kumar<sup>1</sup> and Hamza Varikoden<sup>2</sup>

The Earth's surface temperatures have increased significantly since the beginning of industrialisation. The high emissions of greenhouse gases have contributed to global warming and climate change, which is expected to continue. Here, we investigate the long-term trends of surface temperature in India using surface, satellite and reanalysis data for the period of 1980–2020, and assess the influence of geophysical drivers on temperature change using the causal discovery. The highest mean surface temperatures are observed in the southern India and the lowest in Himalaya in accordance with the incidence of solar radiation. Causal discovery reveals the relative influence of atmospheric processes, aerosols and specific humidity on surface temperature. We observe a positive trend in temperature during pre-monsoon ( $0.1\text{--}0.3\text{ }^{\circ}\text{C dec}^{-1}$ ) and post-monsoon ( $0.2\text{--}0.4\text{ }^{\circ}\text{C dec}^{-1}$ ) seasons in the northwest, northeast and north-central India. The analysis exposes high annual ( $0.22 \pm 0.14\text{ }^{\circ}\text{C dec}^{-1}$ ) and monsoon ( $0.24 \pm 0.08\text{ }^{\circ}\text{C dec}^{-1}$ ) warming in the northeast India. Post-monsoon season shows a positive trend in the entire India, where the highest value is estimated for the western Himalaya ( $0.2\text{--}0.5\text{ }^{\circ}\text{C dec}^{-1}$ ) and northeast India ( $0.1\text{--}0.4\text{ }^{\circ}\text{C dec}^{-1}$ ). Analyses with the Coupled Model Intercomparison Project 6 (CMIP6) results show that temperature can increase up to  $1.1\text{--}5.1\text{ }^{\circ}\text{C}$  by year 2100 under the Shared Socioeconomic Pathways (SSP5)–8.5 scenario. The increasing trend of temperature in India is a big concern, which calls for adaption and mitigation measures to alleviate adverse effects of accelerated warming and regional climate change.

*npj Climate and Atmospheric Science* (2023) 6:164; <https://doi.org/10.1038/s41612-023-00494-0>

## INTRODUCTION

Surface temperature is the key component of the Earth's energy balance, and its change decides weather and climate of a region<sup>1</sup>. Human-caused greenhouse gas (GHG) emissions have increased significantly since the pre-industrial era, causing earth's atmosphere to warm<sup>2,3</sup>. The global surface temperature is expected to increase up to  $1.4\text{--}5.8\text{ }^{\circ}\text{C}$  by the end of twenty-first century, which would likely to increase the magnitude and frequency of extreme events such as heat waves, droughts, increased precipitation and wildfires<sup>3,4</sup>. Several studies have already been conducted to examine the impact of climate change and its influence on extreme weather events<sup>5,6</sup>.

The study of temperature variability requires special attention since the warming is not uniform across the latitudes<sup>7,8</sup>. During the twentieth century, the worldwide mean surface air temperature has increased by around  $0.5\text{ }^{\circ}\text{C}$ <sup>3,9,10</sup>. Analysis and monitoring of air temperature on global and regional scales have attracted a lot of attention in recent decades due to apparent indicators of widespread warming and climate change. As a result, much importance has been given to regional temperature change as that would affect the weather and climate of the regions<sup>2</sup>.

According to previous studies, India's surface temperature has significantly increased during the past two decades<sup>7,11,12</sup>. The annual minimum temperature shows a rise in most parts of India at  $0.24\text{ }^{\circ}\text{C dec}^{-1}$  from 1980 to 2010<sup>13</sup>, demonstrating a significant exacerbation in surface temperatures<sup>14,15</sup>. A positive trend in the diurnal range of temperature has been observed over India from 1901 to 2003<sup>7,16</sup>. South India shows relatively more warming<sup>17</sup>, which is contributed by the rising maximum ( $1\text{ }^{\circ}\text{C }100\text{ yr}^{-1}$ ) and minimum ( $0.3\text{ }^{\circ}\text{C }100\text{ yr}^{-1}$ ) surface temperatures during the period 1901–2007. Many studies on the surface urban heat island intensity suggested that urbanisation can be a reason for the rise

in temperature in Indian cities<sup>18,19</sup>. Dimri<sup>20</sup> also reported a notable warming in India and its sub-regions by using gridded data from the India Meteorological Department (IMD) and reanalysis data sets.

According to Kothawale and Kumar<sup>7</sup>, the average annual maximum temperature has increased by around  $0.07\text{ }^{\circ}\text{C dec}^{-1}$  from 1901 to 2003, whereas the minimum temperature showed no change. Srivastava et al.<sup>21</sup> examined decadal changes in surface temperature of India, and found widespread cooling and warming in the southern and northern India, respectively. Although the trends in mean temperature over India were identical to hemispheric and global trends, Rupa Kumar et al.<sup>22</sup> noted that the diurnal asymmetry of surface temperature across India varied significantly from that recorded elsewhere in the world. Krishnan and Ramanathan<sup>23</sup> assert that surface temperature from January to May decreased up to  $0.3\text{ }^{\circ}\text{C}$  in India during the period 1968–1997, after excluding the impact of GHGs and natural variability from the data. According to Kothawale and Rupa Kumar<sup>7</sup>, India's annual minimum and maximum temperatures have also increased significantly in 1971–2003. As analysed by Kothawale et al.<sup>8</sup>, the all-India mean, maximum and minimum temperatures have increased by  $0.51$ ,  $0.71$  and  $0.27\text{ }^{\circ}\text{C}$  per 100 year, respectively, from 1901 to 2007, with an accelerated warming during the period of 1971–2007.

Causal discovery has emerged as a prevalent approach in recent studies to understand the teleconnections among different climate parameters. For example, Runge et al.<sup>24</sup> revealed causal relationship between geophysical drivers and land air temperature in specific regions like British Columbia. They found that the causal discovery well detected the teleconnection between monthly climate index Niño (3.4 region) and temperature variability in these regions at a significance level of 5% within a maximum lag

<sup>1</sup>CORAL, Indian Institute of Technology Kharagpur, Kharagpur 721302, India. <sup>2</sup>Indian Institute of Tropical Meteorology, Ministry of Earth Sciences, Pashan, Pune 411008, India.  
✉email: jayan@coral.iitkgp.ac.in

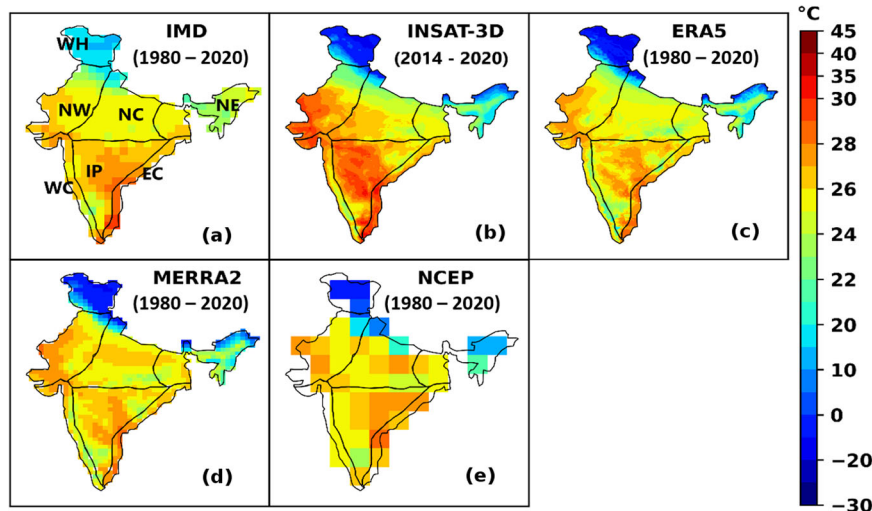


**Fig. 1 Mean surface temperature distribution.** Climatology of mean surface temperature over India derived from the **a** IMD (1980–2020), **b** INSAT (2014–2020), **c** ERA-5 (1981–2020), **d** MERRA-2 (1980–2020) and **e** NCEP (1980–2020) data.

of 6 months. Furthermore, Chu et al.<sup>25</sup> employed the structure learning techniques to identify the causal relationships among the geospatial indices concerning sea surface temperature and pressure. This study concentrated on improving the conventional causal discovery approach, such as the Peter and Clark (PC) algorithm introduced by Spirtes and Glymour<sup>26</sup>. The objective of these studies is the development of causal models based on nonlinear time series data, which are more helpful in understanding the cause-effect relationships underlying geophysical drivers and temperature dynamics. Therefore, due to the dearth of studies on temperature variations across the Indian subcontinent for the past decade, we examine the surface temperature in India for the period of 1980–2020 using surface, satellite, model projections and reanalyses data by applying a suite of statistical tools, including causal discovery.

## RESULTS AND DISCUSSION

### Climatology of surface temperature

The climatology of mean temperature over India is found from the surface measurements of IMD and reanalysis data for the period of 1980–2020. The mean temperature over India from the Indian National Satellite System (INSAT)-3D measurement is also estimated for the period 2014–2020 (Fig. 1). We use the IMD measurements as the reference, in order to assess the robustness of our analysis (Supplementary Fig. 1). Furthermore, the gridded surface data are validated using IMD station measurements from Bangalore, Indore, Silchar and Pune, as demonstrated in Supplementary Figs. 2 and 3. Surface measurements from IMD show a temperature range of about 15–30 °C in India (Fig. 1a). Parts of East Coast (EC), Interior Peninsula (IP) and West Coast (WC) show a higher mean temperature of 30 °C, whereas Western Himalaya (WH) shows a lower value of 15 °C. The Northwest (NW), North Central (NC) and Northeast (NE) regions show a similar temperature range of 21–26 °C. INSAT-3D shows that the west and south of India have warmed more than the rest of the country, as it represents the average surface temperature for the past decade (Fig. 1b). The EC, IP, WC and NW regions show a higher mean temperature of 31 °C in the satellite measurements. This difference between INSAT-3D and IMD can be due to the different time period and spatial resolution. Therefore, we regressed the data to  $1^\circ \times 1^\circ$  by using bilinear interpolation, as IMD measurements are taken as the reference data (Supplementary Figs. 4–6). We compare the temperature measurements for the common time period, as shown in Supplementary Fig. 7. The reanalysis data

show similar temperature distribution throughout India. Temperatures in most parts of NC, NE and NW range from 10° to 30 °C, as found in Fig. 1c–e. The reanalyses data show a range of 24–30 °C in WC, consistent with that of IMD. Some parts of EC show a temperature range of about 25–30 °C in the reanalysis, as shown by the IMD data. The reanalysis data show lower values in some regions of WH. Shifts in equipment, measurement altitude and position can affect observation precision and consistency, and are the reasons for the differences<sup>27</sup>.

### Seasonal distribution of surface temperature

Figure 2 shows the surface temperature distribution for the post-monsoon (October–November; ON), monsoon (June–July–August–September; JJAS), winter (December–January–February; DJF) and pre-monsoon (March–April–May; MAM) seasons as derived from the IMD and reanalyses data. In winter (Fig. 2m), surface temperature from IMD shows a range of 4–32 °C across India, with lower temperature in the hilly regions. The NC, NW and NE regions show temperatures from 15 to 24 °C in this season, as observed from the IMD measurements. Most of the NC, NE and NW regions show similar temperature range (10–22 °C) as analysed from IMD and all other data sets. In contrast to NW, NE, NC and WH, the IP and coastal regions of EC and WC show higher temperature variability in winter. The pre-monsoon season shows high temperature (24–32 °C) in South India (Fig. 2a). The temperatures in EC show about 28–32 °C in this season. The coastal regions and parts of NC and NW show a higher mean surface temperature of 36 °C. In monsoon season, parts of NW show high values of about 32 °C as found from the IMD measurements, which is smaller than the reanalysis data by 2–3 °C (Fig. 2e). Parts of EC show a high mean surface temperature of 26–30 °C as found from the IMD data, which is in agreement with all reanalysis data. In post-monsoon season, parts of NC, NE and NW show similar temperature variation (15–25 °C) in IMD and other data sets (Fig. 2i). Reanalysis data show similar temperature variation, in accordance with the IMD measurements, as demonstrated in Fig. 2 (second, third and bottom panels from top).

### Inter-annual variability in surface temperature

Figure 3a–h shows the temperature anomalies derived from IMD, INSAT-3D and reanalysis data with respect to their respective climatological mean for the period 1980–2020. As observed from the IMD data, India experienced relatively higher temperature in

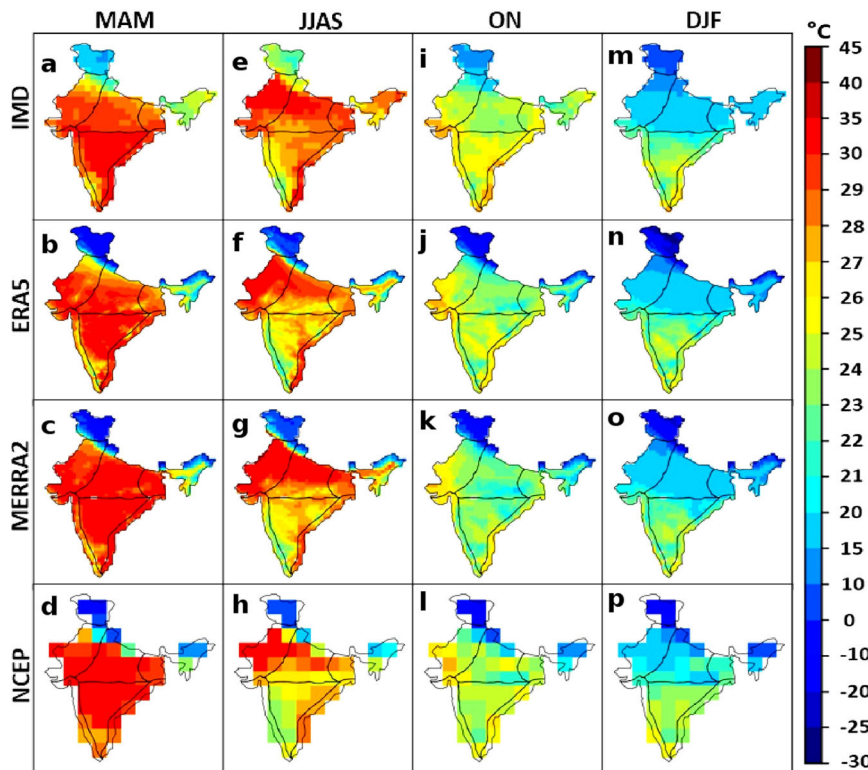


**Fig. 2 Seasonal surface temperature distribution.** Mean surface temperature over the period 1980–2020 in India as analysed using India Meteorological Department (IMD) measurements, NCEP, MERRA-2 and ERA-5 reanalysis data for **a–d** pre-monsoon (MAM), **e–h** monsoon (JJAS), **i–l** post monsoon (ON) and **m–p** winter (DJF). Here, MAM is March–April–May, JJAS is June–July–August–September, ON is October–November and DJF is December–January–February.

2009, 2010, 2015 and 2016. This may be attributed to the short-term variability induced by El Niño events<sup>28,29</sup>. The drop in temperature from 1982 to 1983 in India may be attributed to the volcanic eruption of El Chichón and associated aerosols in the atmosphere<sup>30</sup>. A similar situation is observed from 1991 to 1992 in India, after the eruption of Mount Pinatubo. Among the regions, WH (Fig. 3a) shows high anomaly in surface temperatures from 2015 to 2016 followed by the NE region (Fig. 3f), which could be due to the effect of El Niño during the period. The five warmest years in the past 15 years on record are 2016, 2009, 2017, 2010 and 2021 and thus, these years show relatively higher temperature anomalies. Although there are spatial differences, all regions show an increase in mean surface temperature from 1980 to 2020.

NC and NE show similar temperature changes from 1980 to 2020. A positive temperature anomaly is observed during the super El Niño years 1997–1998 and 2015–2016, particularly in EC, IP, WH and NW (Fig. 3). A relatively higher temperature anomaly during these events is also observed in other parts of the world like East Asia and Western Pacific<sup>31,32</sup>. The rise in temperature in 2002, 2003, 2009 and 2010 can be due to the El Niño events<sup>33</sup>. According to National Oceanic and Atmospheric Administration (NOAA), the year 2016 with El Niño was the warmest<sup>34</sup>. The years 2019 and 2020 were the seventh and eighth warmest on the record until 2020 (IMD Press release, 2020). Some major extreme events, such as heat waves in Maharashtra (western India), Bihar and Jharkhand (eastern India) also occurred in 2019 and 2020. Similar variability is also found in other data sets, as in IMD, across all regions (e.g. the anomalies in volcanic eruption and El Niño periods).

#### Long-term trends in surface temperature

We have also estimated the trends in temperature using the IMD and reanalysis data, and are shown in Fig. 4a–p. In general, IMD

data reveal consistent and statistically significant temperature trends across the distinct regions and seasons (Fig. 4a, e, i, m). Specifically, in pre-monsoon, post-monsoon and winter seasons, NW, NE, WH, WC and IP show positive trends within  $0.1\text{--}0.2\text{ }^{\circ}\text{C dec}^{-1}$ . During monsoon (Fig. 4e), NE shows a consistent warming with positive trends of  $0.1\text{--}0.2\text{ }^{\circ}\text{C dec}^{-1}$ . There are significant annual warming trends of  $0.22 \pm 0.12\text{ }^{\circ}\text{C dec}^{-1}$  within NE, and these patterns persist during monsoon with values of about  $0.25 \pm 0.03\text{ }^{\circ}\text{C dec}^{-1}$ . However, in monsoon season, significant trends in temperature emerge across various regions, such as the east and west coasts, at about  $0.08 \pm 0.06$  and  $0.09 \pm 0.06\text{ }^{\circ}\text{C dec}^{-1}$ , respectively. Furthermore, we observe that the pre-monsoon temperature trends (Fig. 4a) exhibit the highest values in NW ( $0.34 \pm 0.22\text{ }^{\circ}\text{C dec}^{-1}$ ), whereas the lowest in EC ( $0.09 \pm 0.1\text{ }^{\circ}\text{C dec}^{-1}$ ). Additionally, during post-monsoon (Fig. 4i), NW experiences the most pronounced warming of about  $0.24 \pm 0.16\text{ }^{\circ}\text{C dec}^{-1}$ , but EC exhibits the lowest of about  $0.16 \pm 0.08\text{ }^{\circ}\text{C dec}^{-1}$ . These findings further emphasise the regional variability and distinct warming patterns prevalent during different seasons; contributing to a nuanced understanding of temperature trends across India.

In a similar study, Kothawale et al.<sup>8</sup> analysed the trends in surface temperature based on the IMD station data for the period of 1971–2007, and our results are in accordance with their analysis for all seasons. For example, they found statistically significant positive trends in the homogeneous regions such as NW ( $0.034\text{ }^{\circ}\text{C yr}^{-1}$ ), NC ( $0.025\text{ }^{\circ}\text{C yr}^{-1}$ ), NE ( $0.027\text{ }^{\circ}\text{C yr}^{-1}$ ), WC ( $0.027\text{ }^{\circ}\text{C yr}^{-1}$ ), EC ( $0.020\text{ }^{\circ}\text{C yr}^{-1}$ ), WH ( $0.068\text{ }^{\circ}\text{C yr}^{-1}$ ) and IP ( $0.018\text{ }^{\circ}\text{C yr}^{-1}$ ) for winter and NE ( $0.018\text{ }^{\circ}\text{C yr}^{-1}$ ) for monsoon season. Our findings are consistent with these results and the differences in trend values are mainly due to the differences in time period and horizontal resolution of data sets.

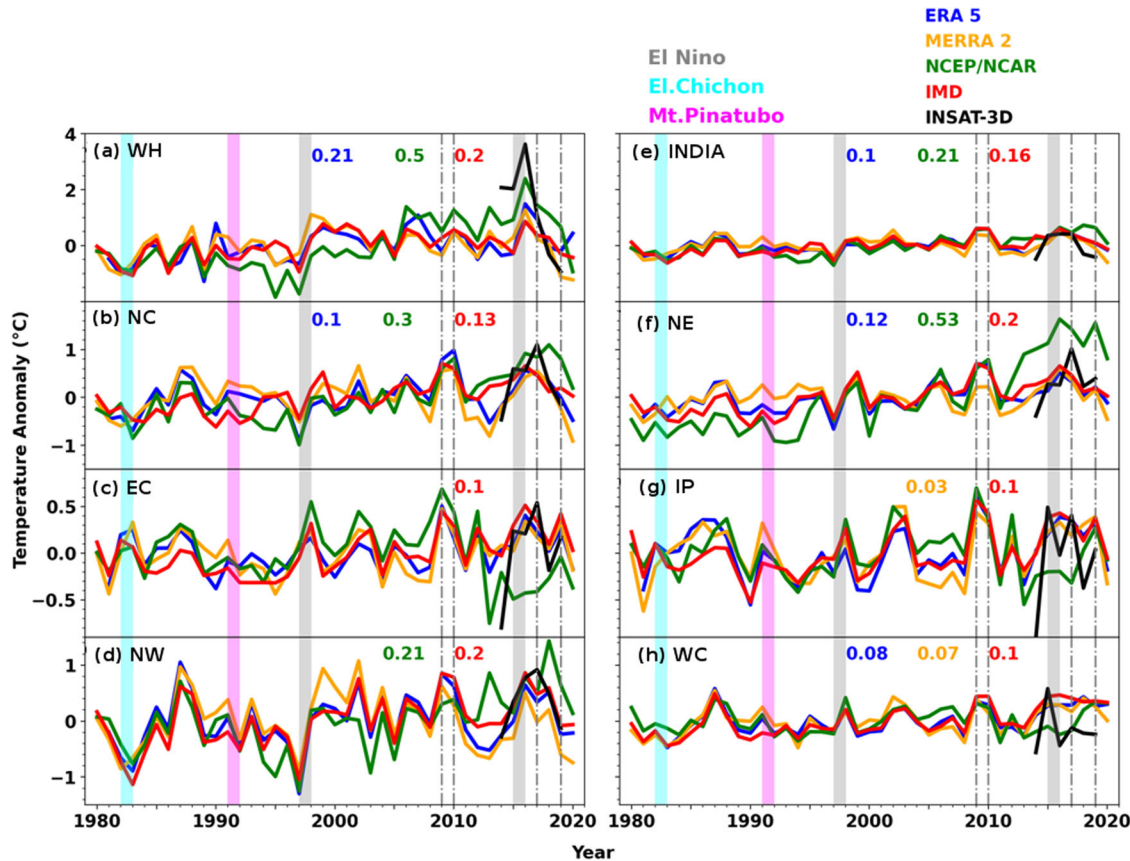


**Fig. 3 Temperature evolution over the homogenous regions. a–h** Temperature anomalies averaged over the homogeneous regions for the period of 1980–2020. The anomalies are computed with respect to the baseline period of 1980–2020 from IMD, ERA-5, MERRA-2 and NCEP/NCAR data. The INSAT-3D data are analysed from 2014 to 2019. The vertical dashed lines represent the rise in temperature due to the warmest years of 2009, 2010, 2017 and 2019, which are second, third, fourth and seventh warmest on record, respectively, until 2020. The trend (per decade) values of each time series are denoted in numeric (statistically significant at the 95% CI). The linear trend values are shown in the same colour text in the respective panels. The statistically significant values are marked with a star sign. Here, NW is Northwest, WH is Western Himalaya, NC is North Central, NE is Northeast, EC is East Coast, WC is West Coast and IP is Interior Peninsula. The super El Niño years (1997/98 and 2015/16) are shown in grey stripes and the volcanic years are shown in coloured stripes.

According to National Centers for Environmental Prediction (NCEP) and Modern-Era Retrospective analysis for Research and Applications (MERRA)-2 reanalysis data, the WC and IP regions show a significant warming of  $0.1\text{--}0.3\text{ }^{\circ}\text{C dec}^{-1}$  in monsoon season. MERRA-2 data reveal a significant negative trend of about  $-0.2 \pm 0.14\text{ }^{\circ}\text{C dec}^{-1}$  in NW, which can be attributed to the water added to land during monsoon that shifts the Bowen ratio from sensible to latent heating, and thereby cooling the land surface<sup>35,36</sup>. In NCEP, a significant warming of about  $0.1\text{--}0.3\text{ }^{\circ}\text{C dec}^{-1}$  is estimated in monsoon season across most regions in India, which is in contrast to the IMD data.

In pre-monsoon season, the European Centre for Medium-Range Weather Forecasts (ECMWF) Re-Analysis (ERA)-5 data show an increase in temperature in parts of WH, NW, WC and NE, which are in agreement with the IMD measurements (Fig. 4b). MERRA-2 data show significant warming in some areas of WC, NW and NE. IMD and ERA-5 data also show a similar trend in monsoon season. In winter, the ERA-5 data in IP, NE and coastal regions show a warming trend, which is  $0.1\text{--}0.2\text{ }^{\circ}\text{C dec}^{-1}$ , slightly higher than that of IMD measurements (Fig. 4n). Also, a negative trend of  $-0.2$  to  $-0.4\text{ }^{\circ}\text{C dec}^{-1}$  is estimated in parts of NE, IP and EC from the MERRA-2 data. The post-monsoon season accounts for much of the warming in India, and the highest warming is observed in WH, NC and NE, as analysed from the ERA-5 and NCEP data. The IMD and reanalysis data exhibit a significant warming ( $0.1\text{--}0.4\text{ }^{\circ}\text{C dec}^{-1}$ ) in NE in this season.

We have also looked at the temporal evolution of surface measurements of IMD for the past four decades (1980–2020) and the previous three decades (1990–2020) and found a statistically significant surge in  $T_{\max}$ ,  $T_{\min}$  and  $T_{\text{mean}}$  across India during 1990–2020 as compared to that in 1980–2020. The trends estimated from the all-India averaged annual and seasonal surface maximum temperature ( $T_{\max}$ ), minimum temperature ( $T_{\min}$ ) and mean temperature ( $T_{\text{mean}}$ ) data are listed in Supplementary Table 2. In addition, we have examined the decadal changes in  $T_{\max}$ ,  $T_{\min}$  and  $T_{\text{mean}}$  trends from the IMD measurements for the period 1980–2020, and are shown in Supplementary Table S3.

As found with  $T_{\text{mean}}$ , a similar variation is also observed in  $T_{\min}$  and  $T_{\max}$  over India for the period 1980–2020, as shown in Fig. 5a–h. For instance, high values of  $T_{\max}$  and  $T_{\min}$  in 1997, 2002, 2003, 2009, 2010 and 2016 in all regions can be attributed to the El Niño events in those years. The drop of  $T_{\min}$  and  $T_{\max}$  in 1982 and 1991 is due to the aerosols loading from the El Chichon and Mount Pinatubo eruptions, respectively. During the volcanic eruptions, huge amount of sulphate aerosols is emitted into the atmosphere. Due to the scattering nature of these particles, they reflect the incoming solar radiation, hence, cool the earth surface<sup>37,38</sup>. Other than the annual variability, a gradual increase in  $T_{\min}$  and  $T_{\max}$  is observed in all regions since 1995. The rate of rise in  $T_{\min}$  is very high in NW ( $(0.27 \pm 0.10)\text{ }^{\circ}\text{C dec}^{-1}$ ), WC ( $(0.15 \pm 0.06)\text{ }^{\circ}\text{C dec}^{-1}$ ), NC ( $(0.17 \pm 0.06)\text{ }^{\circ}\text{C dec}^{-1}$ ) and NE ( $(0.23 \pm 0.14)\text{ }^{\circ}\text{C dec}^{-1}$ ) in the past four decades, which is higher

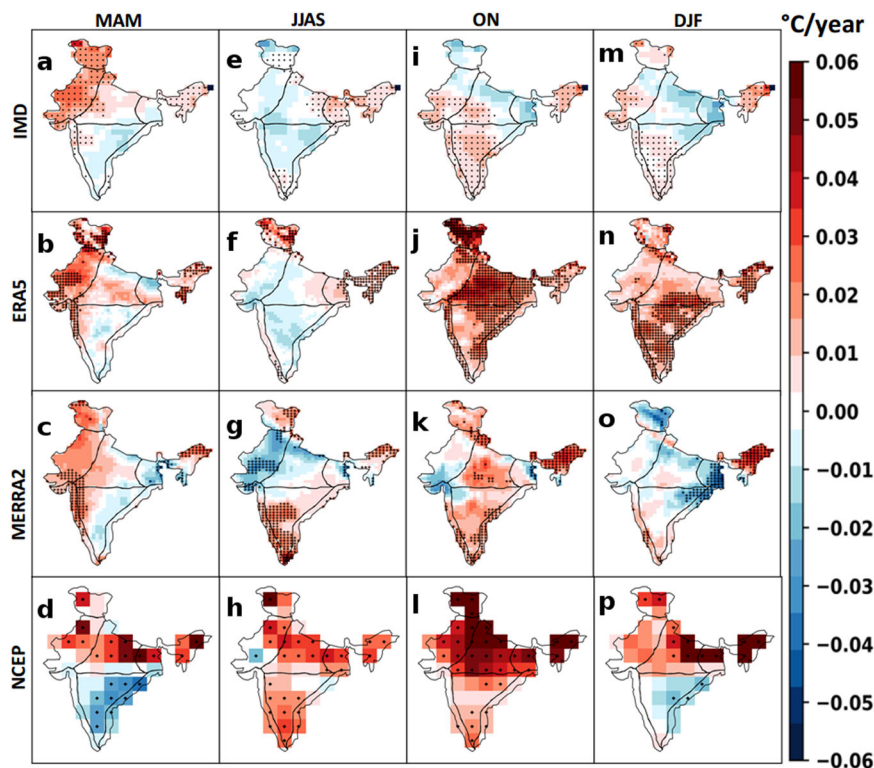


**Fig. 4 Long term trends.** Mean surface temperature ( $T_{\text{mean}}$ ) trends over India for the period 1980–2020 as analysed using India Meteorological Department (IMD) measurements, NCEP, MERRA-2 and ERA-5 reanalysis data for **a–d** pre-monsoon (MAM), **e–h** monsoon (JJAS), **i–l** post monsoon (ON) and **m–p** winter (DJF). The hatched areas represent statistically significant trends at the 95% confidence interval. Here, MAM is March–April–May, JJAS is June–July–August–September, ON is October–November and DJF is December–January–February.

than the rate of increase of  $T_{\text{max}}$ ; indicating the slow background warming in India. Similarly, the rate of rise of  $T_{\text{max}}$  is higher than the  $T_{\text{min}}$  in EC, IP and WH; suggesting the impact of rise in humidity and henceforth, temperature in those coastal and hilly regions.

There are seasonal differences in the temporal evolution of  $T_{\text{min}}$  and  $T_{\text{max}}$  over the regions, as can be observed from Supplementary Fig. 11 to 14. During pre-monsoon, a gradual decrease in both  $T_{\text{max}}$  and  $T_{\text{min}}$  is found in NC, NW, WH, NE and all India, particularly after 2010. In winter, all regions show a rise in  $T_{\text{min}}$  and  $T_{\text{max}}$  in the past four decades, with a high rise of  $T_{\text{min}}$  in NW ( $0.3 \pm 0.16^{\circ}\text{C dec}^{-1}$ ) and WC ( $0.18 \pm 0.08^{\circ}\text{C dec}^{-1}$ ). On the other hand, the rate of increase of  $T_{\text{max}}$  is higher in IP ( $0.25 \pm 0.12^{\circ}\text{C dec}^{-1}$ ), WH ( $0.23 \pm 0.20^{\circ}\text{C dec}^{-1}$ ) and EC ( $0.23 \pm 0.08^{\circ}\text{C dec}^{-1}$ ) as compared to that of  $T_{\text{min}}$ . During post-monsoon, the difference in rate of rise in  $T_{\text{min}}$  and  $T_{\text{max}}$  is very high in NW ( $0.31^{\circ}\text{C dec}^{-1}$ ) and NC ( $0.15^{\circ}\text{C dec}^{-1}$ ). In monsoon, more pronounced rise in  $T_{\text{max}}$  ( $0.24 \pm 0.08^{\circ}\text{C dec}^{-1}$ ) and  $T_{\text{min}}$  ( $0.21 \pm 0.06^{\circ}\text{C dec}^{-1}$ ) is observed in NE, in contrast to other regions. Also, the rate of rise in  $T_{\text{min}}$  in NW ( $0.17 \pm 0.08^{\circ}\text{C dec}^{-1}$ ) and NC ( $0.12 \pm 0.06^{\circ}\text{C dec}^{-1}$ ) is significantly higher as compared to that of  $T_{\text{max}}$  [NW ( $0.001 \pm 0.16^{\circ}\text{C dec}^{-1}$ ) and NC ( $0.08 \pm 0.16^{\circ}\text{C dec}^{-1}$ )]. In brief, the regional and seasonal assessment of temporal evolution of mean, maximum and minimum temperature for the period 1980–2020 suggest a gradual rise in surface temperature in India.

Increased GHG emissions are causing global warming, as shown by rising global mean surface temperatures<sup>39</sup>. However, due to changes in the land use and cover, such as urbanisation<sup>36,40,41</sup>, regional surface temperature may have varying trends<sup>27,42</sup>. Our analyses find significant warming in India in most seasons and regions, which is consistent with a previous study for the period 1901–2003 by Pal and Al-Tabba<sup>11</sup>. Surface temperature of India has increased during past four decades across the regions, and

thus, it can have large implications on extreme events like heat waves. Rohini et al.<sup>15</sup> found that the frequency, duration and intensity of heat waves have increased in India during the period 1961–2013. Pai et al.<sup>43</sup> have found that the frequency of heat waves in India has enhanced during 1961–2010. Sharma and Mujumdar<sup>44</sup> observed an increasing frequency of heat waves in NW, IP, NE and some parts of west central India during the period 1951–2010, and their frequency was higher in 1981–2010 due to the global warming. As per the CMIP5 projections, heat waves happen during March–June in India would be more frequent with increased intensity and prolonged duration, and may occur earlier in the year<sup>45</sup>. Krishnan et al.<sup>29</sup> reported that the mean duration of summer heatwaves in India under the RCP8.5 (Representative Concentration Pathway 8.5) scenario is significantly longer than that projected under RCP4.5, with approximately 25 and 35 heatwave days per season by the mid and end of twenty-first century, respectively. These findings are in agreement with the CMIP5 model results<sup>46</sup>.

#### Multiple linear regression of mean surface temperature

We have also used a Multiple Linear Regression (MLR) model to find the trends of surface temperature in different regions of India<sup>47</sup>. The normalised predictors used in the model are Aerosol Optical Density (AOD) at 550 nm derived from MERRA-2, El-Nino Southern Oscillation (ENSO) index, solar flux (SF), specific humidity (SH) and Tropopause Height (TPH) from MERRA-2, Dipole Mode Index (DMI) to find the influence of Indian Ocean Dipole (IOD) and cloud cover from ERA-5. We have also given an additional lag of 3 months for ENSO and solar flux. Supplementary Fig. 15 shows the correlation matrix of different predictors used. We have computed the Variation Inflation Factor (VIF) to find the variance of these proxies and their correlation. The VIF values vary between 1 and 1.57, which indicate that the predictors used are not highly

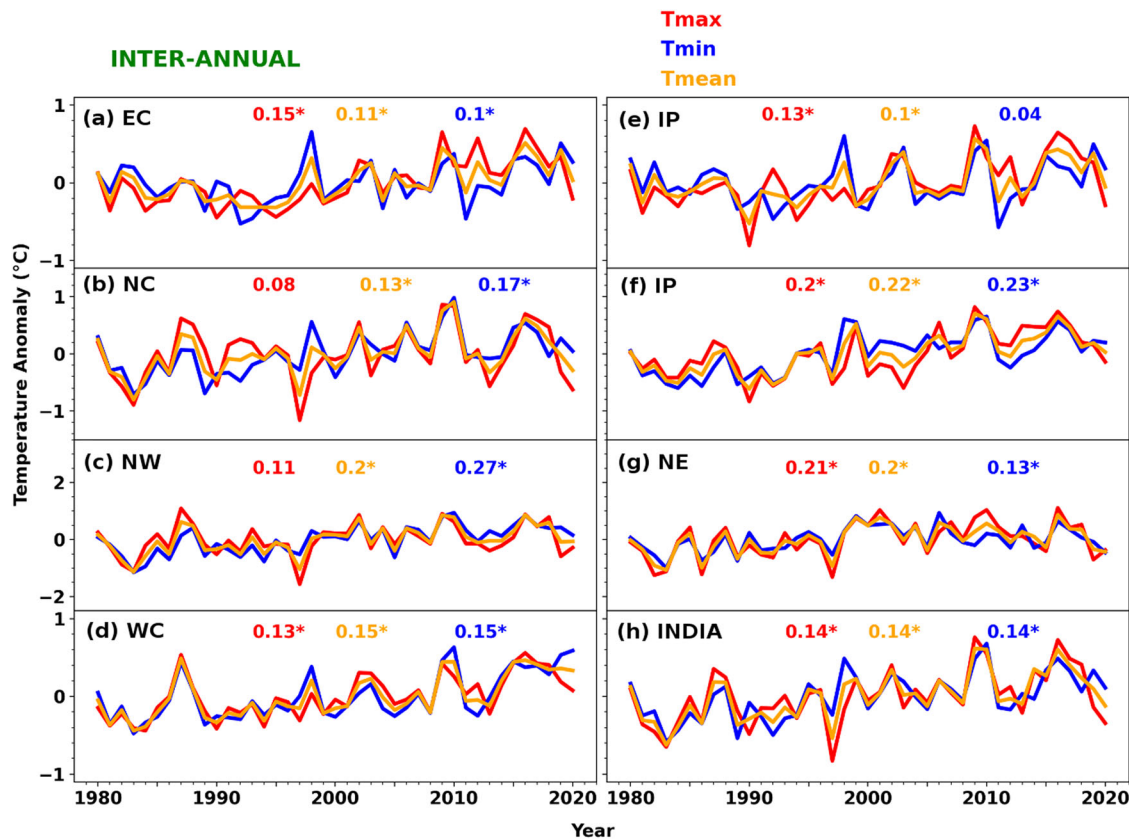


**Fig. 5 Minimum and Maximum temperature changes.** a–h Annual averaged maximum ( $T_{\max}$ ), temperature ( $T_{\min}$ ) and mean ( $T_{\text{mean}}$ ) temperature from the IMD data in the temperature homogenous regions and entire India from 1980 to 2020. The numbers at top of each panel represent the temperature trends ( $^{\circ}\text{C}$  per decade) and the star indicates that values are statistically significant at the 95% CI. Here, NW is Northwest, WH is Western Himalaya, NC is North Central, NE is Northeast, EC is East Coast, WC is West Coast and IP is Interior Peninsula.

correlated to each other. Supplementary Fig. 16 shows the normalised MLR fit of temperature at different regions of India for the period 1980–2020. The regressed time series fits the observed temperature data with high  $R^2$  values ( $>0.7$ ), except for IP and NC (about 0.5). The trends computed with MLR are in agreement with those by the linear regression using the IMD data and are within  $0.05$ – $0.25\text{ }^{\circ}\text{C dec}^{-1}$  in all homogenous regions (Fig. 5). The trends estimated using MLR are about  $0.16\text{ }^{\circ}\text{C dec}^{-1}$  for the coastal regions (EC and WC) and  $0.15\text{ }^{\circ}\text{C dec}^{-1}$  for NW and NE regions.

#### Causal discovery of geophysical drivers of surface temperature

The causal analysis shows distinct difference in the impact of various processes on the surface temperature among the regions (Fig. 6a–g). For instance, precipitation and SH impact positively, whereas Heat Flux (HF) affects temperature negatively in real time in EC and NC with a cross-correlation greater than 0.4. Similarly, SH and precipitation are positively cross-correlated to temperature in NW and IP, with a conditional-correlation greater than 0.4. Water vapour is one of the most abundant GHGs in the atmosphere that can enhance the temperature<sup>48</sup>, which can be the reason for the direct association of SH to temperature in these regions. In addition, the rise in temperature influences SH through evapotranspiration, where temperature impacts SH in real time. ENSO affects TPH positively in all regions, except in WH. Similarly, TPH affects temperature positively in WH, with a cross-correlation of about 0.3 (Fig. 6g). This can be due to the higher altitudes, where tropopause height directly influences temperature. No direct relation is observed between ENSO and temperature in any region. DMI influences precipitation in WC, which indirectly affects

the temperature with positive correlation of 0.8 (Fig. 6f). Furthermore, precipitation and temperature are positively correlated in all regions, with a coefficient of about 0.8. This suggests that higher temperature owing to global warming and climate change can lead to extreme precipitation events<sup>49,50</sup>. HF influences temperature negatively in NC ( $-0.3$ ) with lag of 3 months (Fig. 6c). Some regions also show a direct relation of precipitation with SH, e.g., NC, NE and WH have a positive correlation, as shown in Fig. 6. It can be elucidated by the process of cloud formation, wherein moisture condenses, resulting in precipitation. Conversely, precipitation contributes a substantial volume of water to the Earth's surface and consequently increases atmospheric moisture through evaporation and evapotranspiration driven by temperature<sup>51</sup>. The edges without arrow in causal analysis imply an association between the drivers. Nevertheless, there could potentially exist an instantaneous causal relationship, which depends on the available measurements to establish a statistical relationship between the drivers. Note that, this connection might not have deemed to be unequivocally causal.

#### Projection of surface temperature by CMIP6 models

Here, the selection of models is based on their data availability for the historical (1980–2014) and three Shared Socioeconomic Pathways (SSP) scenarios (SSP1-2.6, SSP2-4.5 and SSP5-8.5 from 2015 to 2099) along with their performance over India in the present climate against the IMD observations. For the projected changes of temperatures in future, the period 2015–2099 is divided into near (2030–2049), mid (2060–2079) and far (2080–2099) future. From the CMIP6 models, we selected 3 models (Model for Interdisciplinary Research on Climate (MIROC) 6

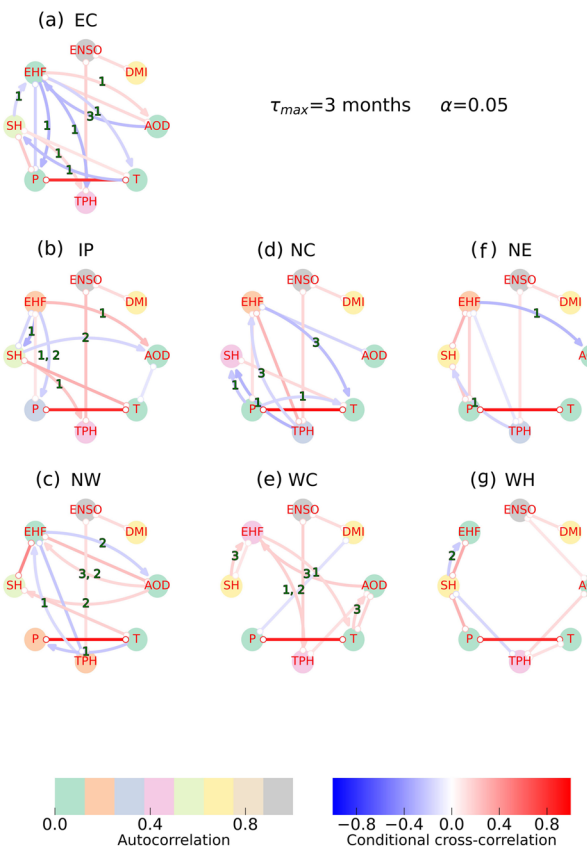


**Fig. 6 Causal discovery of surface temperature.** a–g Causal discovery of surface temperature with its drivers for different homogeneous regions of India with maximum allowable lag of 3 months at the 95% CI. Here, NW is Northwest, WH is Western Himalaya, NC is North Central, NE is Northeast, EC is East Coast, WC is West Coast and IP is Interior Peninsula. The drivers are shown in the solid circles (e.g. EHF is eddy heat flux, SH is specific Humidity, P is precipitation and T is temperature).

Japan; Community Earth System Model (CESM) 2 USA and Community Integrated Earth System Model (CIESM) China) on the basis of least mean bias error (MBE) against the IMD observations.

We have compared the CMIP6 model results with IMD measurements for the present climate period 1995–2014 and estimated the bias between the data sets. The lowest MBE is shown by MIROC6 ( $-0.16^{\circ}\text{C}$ ) followed by CESM2 ( $0.57^{\circ}\text{C}$ ) and CIESM ( $1.01^{\circ}\text{C}$ ), but CNRM-CM6-1HR shows the highest MBE of  $4.95^{\circ}\text{C}$ . Figure 7a–f illustrates the change of temperature in India during the twenty-first century with near (2030–2049), mid (2060–2079) and far (2080–2099) future scenarios with respect to the climatological mean for the baseline period of current climate (1995–2014). The IMD observations are also presented together with historical simulations (1995–2014). The CESM2 (Fig. 7b) and CIESM (Fig. 7c) models show similar changes in temperature with a warming of  $1.3\text{--}3.5^{\circ}\text{C}$  in mid-future and  $1.1\text{--}5.1^{\circ}\text{C}$  in far future periods. As illustrated in Supplementary Table 4, the annual mean temperature in India is projected to increase by  $1.02\text{--}3.3^{\circ}\text{C}$  by the end of twenty-first century in all the three scenarios, as simulated by MIROC6 (Fig. 7a). Chaturvedi et al.<sup>52</sup> showed the mean warming over India under the RCP8.5 scenario to be  $3.3\text{--}4.8^{\circ}\text{C}$  by the 2080s as analysed using 18 CMIP5 models. The enhanced warming in mid ( $1.5\text{--}2^{\circ}\text{C}$  warming world) and far future (more than  $3\text{--}4^{\circ}\text{C}$  warming world) poses a serious threat to the glaciers in Himalaya, and is also likely

to affect the frequency of flash floods, heat waves and wildfires, and thereby making the people more vulnerable to climate change. Therefore, it is crucial to understand and evaluate the changes of temperature in India for improved climate policy decisions.

In sum, a high warming trend is observed in NE during winter and post-monsoon seasons, but pre- and post-monsoon seasons in WH (about  $0.3^{\circ}\text{C dec}^{-1}$ ). The warming in these ecologically sensitive hilly regions is a great concern for snow-melt and water bodies there. The NW region in monsoon season shows a positive trend of  $0.34 \pm 0.22^{\circ}\text{C dec}^{-1}$  in pre-monsoon. Furthermore, post-monsoon season accounts for much of the warming in India, ranging from  $0.1$  to  $0.5^{\circ}\text{C dec}^{-1}$ . The trends computed using the MLR also yield similar results and are in the range of  $0.05\text{--}0.25^{\circ}\text{C dec}^{-1}$  across the homogenous regions of India. The causal discovery reveals that atmospheric processes, aerosols and water vapour influence the variability of surface temperature, depending on regions. For instance, specific humidity influences the temperature directly in EC, IP, NW and WC regions, but heat flux affects the temperature in most regions (except EC, IP, NW and WH). The mean temperature in India has increased since 1980, with a significant enhancement in the maximum ( $0.14\text{--}0.21^{\circ}\text{C dec}^{-1}$ ) and minimum ( $0.1\text{--}0.23^{\circ}\text{C dec}^{-1}$ ) temperatures. In addition, the future projections reveal that the annual mean surface temperature in India is projected to increase by  $1\text{--}5^{\circ}\text{C}$  with respect to the current climate by the end of this century. The rising temperature will likely to increase the frequency and severity of the extreme weather events and snow/glacier melt in the Himalaya and other hilly regions, which will have adverse effect on human health and agriculture of a region with more than 1.4 billion people.

## METHODS

### Data

The IMD maintains about 550 surface observatories nationwide, where measurements of daily surface air temperature are recorded in  $^{\circ}\text{C}$ . The National Data Centre (NDC) compiles, digitises, quality-controls, and archives these data. Daily temperature data from IMD are available on a  $1^{\circ} \times 1^{\circ}$  resolution. The mean monthly surface temperatures of IMD are derived from daily mean temperatures. Daily precipitation data are available at  $0.25^{\circ} \times 0.25^{\circ}$  resolution, which are converted to mean monthly precipitation. INSAT-3D (Indian National satellite system) is a multipurpose geosynchronous satellite with major meteorological payloads, including an imager and a multi-channel sounder. The INSAT-3D surface temperature data are available at a resolution of  $0.1^{\circ} \times 0.1^{\circ}$  from 2014 to 2020<sup>53</sup>.

The monthly average surface temperature data from the ERA-5, MERRA-2 and National Center for Environmental Prediction/National Center for Atmospheric Research (NCEP/NCAR, hereafter NCEP) from 1980 to 2020 are also considered. Reanalysis data sets use robust techniques to combine a variety of land and marine observations, creating a comprehensive data set that encompass both space and time<sup>54</sup>. In regions where in situ measurements are scarce, reanalysis data can be beneficial<sup>12,55</sup>.

The GEOS-5 atmospheric model and data assimilation system and the three-dimensional variational data analysis (3DVAR) Gridpoint Statistical Interpolation meteorological analysis scheme are used to produce MERRA-2<sup>56,57</sup>. The MERRA-2 data have 42 pressure levels from 1000 to 0.01 hPa. The monthly temperature data at a resolution of  $0.625^{\circ} \times 0.5^{\circ}$  from MERRA-2 are considered for our analyses. ERA-5 is the most recent ECMWF reanalysis, that provide hourly, daily and monthly data on many atmospheric, sea-state and land-surface parameters from 1950 onwards, along with uncertainty estimates<sup>58</sup> for 37 vertical pressure levels from surface to 1 hPa. The monthly temperature data at a resolution of

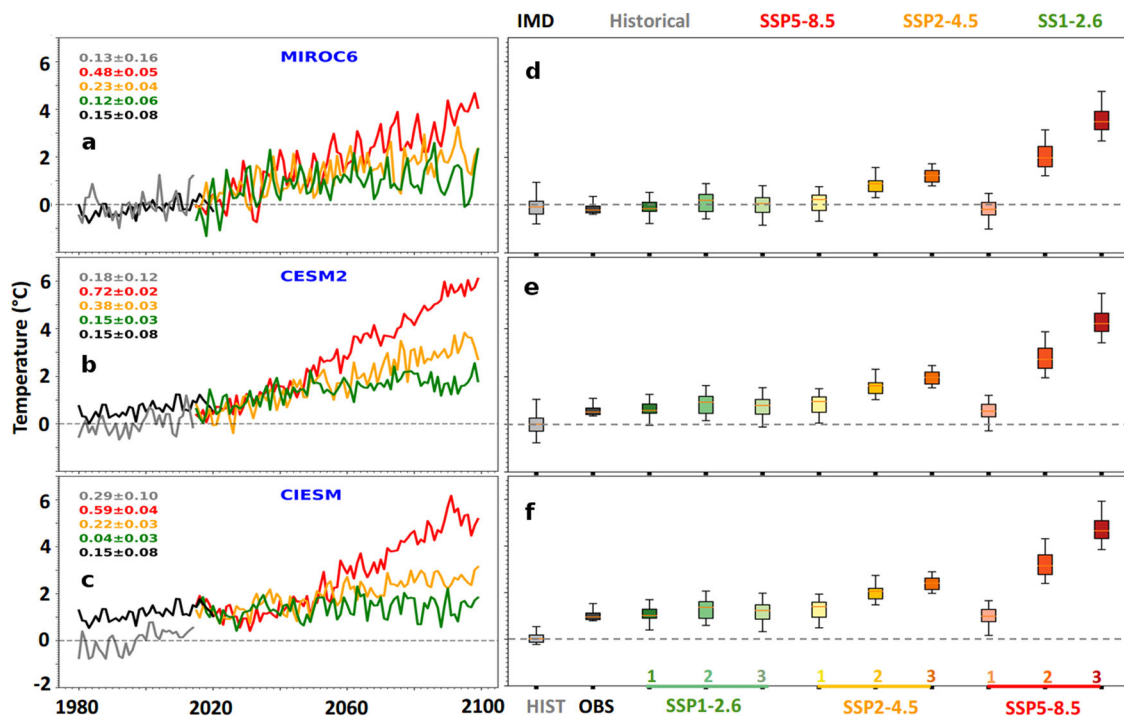


**Fig. 7 Future projections of surface temperature. a–c** The grey, black, red, orange and green curves represent the historical, observation (IMD), and the model projections with respect to the Shared Socioeconomic Pathways SSP5-8.5, SSP2-4.5 and SSP1-2.6 scenarios, respectively. The anomalies are calculated by subtracting each future year value from the climatological mean of the historical period (1995–2014). **d–f** The boxplots represent changes in observation (IMD), near, mid and far-future with respect to the climatological mean for the baseline period of present climate (1995–2014), from all three scenarios of the MIROC6 (Japan), CESM2 (USA) and CIESM (China) model simulations. The numeric 1, 2 and 3 in (d–f) represent the near (2030–2049), mid (2060–2079) and far (2080–2100) future time periods of the SSPs.

$0.25^\circ \times 0.25^\circ$  from ERA-5 reanalysis are used. The NCEP reanalysis project provides atmospheric fields for scientific analyses<sup>59,60</sup>. Data assimilation is carried out using the historical data from 1948 to date, based on a state-of-the-art model<sup>59</sup> on 17 pressure levels from 1000 to 10 hPa. It includes daily and monthly temperature measurements from 1948 onwards. Here, we use the monthly averaged surface (0.995 sigma level) temperature data at a resolution of  $2.5^\circ \times 2.5^\circ$  for the period 1980–2020. The NCEP/DOE reanalysis II provided by NOAA PSL, Boulder, Colorado, USA is available at <https://psl.noaa.gov>.

In this study, we employ various surface temperature data sets, but IMD measurements are taken as the reference to assess the robustness and reliability our analysis (Supplementary Fig. 1). Our comparison shows that the reanalyses data are in good agreement with IMD measurements in all regions, except WH and NE. We also observe a strong positive correlation between the IMD measurements and reanalysis data, with its coefficient  $>0.85$ . However, the correlation is relatively weak for EC, IP, NC and NE in winter, which is about 0.75. For instance, correlation of above 0.85 is found between ERA-5 and IMD in EC, IP, NC and NW regions in all seasons. Similarly, correlation between MERRA-2 and IMD is above 0.75 in EC, IP, NW, NC and WC in pre-monsoon and post-monsoon seasons.

We use the IMD station-based measurements from: Bangalore, Indore, Silchar and Pune (Supplementary Figs. 2 and 3). We compare both  $T_{\min}$  and  $T_{\max}$  data throughout the observation period of these stations. The data exhibit a good correlation with the IMD gridded data, and the correlation is relatively high for minimum temperature, which is greater than 0.96 for all stations. The correlation is slightly small for maximum temperature, within the range of 0.85–0.96. The Root Mean Square Error (RMSE) for maximum temperature lies within the range of 1.4–2.8 °C, whereas it is within 0.9–3.36 °C for minimum temperature.

### Causal discovery

To find the influence of different geophysical drivers on surface temperature (represented as  $T$ ,  $1^\circ \times 1^\circ$  resolution from IMD) distribution, we have considered the following data or indices for representing the respective process in causal analyses. These drivers are the solar flux (SF), Oceanic Niña Index (ONI) for El-Niño Southern Oscillation (ENSO), Eddy heat flux (EHF), Precipitation (represented as  $P$ ,  $0.25^\circ \times 0.25^\circ$  from IMD), Tropopause height (TPH), Dipole mode index (DMI) and Aerosol optical depth (AOD). These data are publicly available from the National Oceanic and Atmospheric Administration Climate Prediction Center (NOAA CPC).

The CMIP6<sup>61</sup> model results analysed in this study are listed in Supplementary Table 1. The CMIP6 data set is obtained from the Copernicus climate data archive where monthly gridded projections of near surface temperatures for integrated Shared Socio-economic Pathway (SSP) represented by SSP1-2.6, SSP2-4.5 and SSP5-8.5 are analysed for the period 2015–2099. We have also analysed the CMIP6 historical data from 1980 to 2014.

Based on the spatio-temporal variability of surface air temperatures throughout the country, India has been conceptually divided into seven temperature homogenous regions for this analysis: east coast (EC), interior peninsula (IP), west coast (WC), north-central (NC), northeast (NE), northwest (NW) and western Himalaya (WH). Trends are estimated using a linear regression method<sup>7</sup>.

We perform the Peter Clark momentary conditional independence (PCMCI) algorithm<sup>24</sup> to understand the causal relation between geophysical drivers and temperature in each region. This algorithm comprises: (i) a condition selection step based on PC algorithm to determine the parents of respective drivers, which perform an iterative conditional independence test by evaluating the partial correlation between two-time series while accounting for other confounding variables with different time lags. In a

causally sufficient condition, it also employs the Markov condition and Faithfulness criteria to construct a range of possible causal links<sup>62</sup>, and (ii) Using the momentary conditional independence (MCI) test, the statistical significance of causal linkages is evaluated before their strength is assessed using a multiple linear regression (MLR).

The PCMCI approach uses a variety of statistical tests, such as Gaussian process regressions and distance correlation (GPDC), conditional mutual information (CMI) and linear partial correlations (ParCorr) to infer causal relationships. The nonparametric test CMI is based on a closest neighbour estimate of conditional mutual information, whereas GPDC is ideal for nonlinear dependency models with additive noise, and is based on Gaussian process regression and a distance correlation test on the residuals. Here, we employ PCMCI, which can also detect contemporary causal links using ParCorr. The PCMCI method has two parameters that can be selected by the user: significance level and maximum time delay, which govern the allowable amount of false-positive link discovery. Detailed discussion on PCMCI can be found in Kumar et al.<sup>63</sup>. Here, stationarity of time series is evaluated using Augmented Dickey–Fuller (ADF) and the Kwiatkowski–Phillips–Schmidt–Shin (KPSS) test before performing causal discovery using PCMCI, and the required time series is made stationary by first order differencing. To account for the impact of climate modes on temperature in Indian regions, we selected 3 months as the maximum allowable time lag. These indices represent mostly the natural forcing with long-term variability, which can influence the surface temperature for a period from a few weeks to several months. For example, during an El Niño, warm sea surface temperature in the tropical Pacific can influence the weather patterns in India, within a time lag of 3 months<sup>64,65</sup>.

## DATA AVAILABILITY

MERRA 2 data are available at <https://disc.gsfc.nasa.gov/>. ERA 5 data are available at <https://cds.climate.copernicus.eu/#/search?text=ERA-5&type=dataset>. NCEP/NCAR reanalysis data is available at <https://psl.noaa.gov/data/gridded/data.ncep.reanalysis.html>. IMD data available at [https://www.imdpune.gov.in/Clim\\_Pred\\_LRF\\_New/Grided\\_Data\\_Download.html](https://www.imdpune.gov.in/Clim_Pred_LRF_New/Grided_Data_Download.html). INSAT-3D data are available at <https://www.mosdac.gov.in/insat-3d-data-products>. CMIP6 data are available at <https://cds.climate.copernicus.eu/#/search?text=ERA-5&type=dataset>. DMI is available at [https://psl.noaa.gov/gcos\\_wgsp/Timeseries/DMI/](https://psl.noaa.gov/gcos_wgsp/Timeseries/DMI/). ENSO MEI index is available at <https://psl.noaa.gov/enso/mei/>. We use an open source python packages, pyINSAT, to read and visualise INSAT data sets (<https://github.com/gopikrishnangs44/pyINSAT>), and pyMLR for MLR analyses (<https://github.com/gopikrishnangs44/pyMLR>) available online via github. All relevant data are available on request.

## CODE AVAILABILITY

The source codes for the analysis of this study are available from the corresponding author on request.

Received: 13 May 2023; Accepted: 6 October 2023;

Published online: 18 October 2023

## REFERENCES

- Barrows, T. T., Juggins, S., De Deckker, P., Calvo, E. & Pelejero, C. Long-term sea surface temperature and climate change in the Australian-New Zealand region. *Paleoceanography* **22**, PA2215 (2007).
- Karl, T. R. & Trenberth, K. E. Modern global climate change. *Science* **302**, 1719–1723 (2003).
- Solomon, S. The physical science basis: contribution of Working Group I to the fourth assessment report of the Intergovernmental Panel on Climate Change. *Clim. Chang.* **2007**, 996 (2007).
- Beniston, M. et al. Future extreme events in European climate: an exploration of regional climate model projections. *Clim. Change* **81**, 71–95 (2007).
- Rind, D., Rosenzweig, C. & Goldberg, R. Modelling the hydrological cycle in assessments of climate change. *Nature* **358**, 119–122 (1992).
- Trenberth, K. E. Conceptual framework for changes of extremes of the hydrological cycle with climate change. *Clim. Change* **42**, 327–339 (1999).
- Kothawale, D. R. & Rupa Kumar, K. On the recent changes in surface temperature trends over India. *Geophys. Res. Lett.* **32**, L18714 (2005).
- Kothawale, D. R., Munot, A. A. & Krishna Kumar, K. Surface air temperature variability over India during 1901–2007, and its association with ENSO. *Clim. Res.* **42**, 89–104 (2010).
- Easterling, D. R. et al. Maximum and minimum temperature trends for the globe. *Science* **277**, 364–367 (1997).
- Jones, P. D. & Moberg, A. Hemispheric and large-scale surface air temperature variations: an extensive revision and an update to 2001. *J. Clim.* **16**, 206–223 (2003).
- Pal, I. & Al-Tabbaa, A. Long-term changes and variability of monthly extreme temperatures in India. *Theor. Appl. Climatol.* **100**, 45–56 (2010).
- Dash, S. K. & Mamgain, A. Changes in the frequency of different categories of temperature extremes in India. *J. Appl. Meteorol. Climatol.* **50**, 1842–1858 (2011).
- Bapuji Rao, B., Santhibhushan Chowdary, P., Sandeep, V. M., Rao, V. U. M. & Venkateswarlu, B. Rising minimum temperature trends over India in recent decades: implications for agricultural production. *Glob. Planet. Change* **117**, 1–8 (2014).
- Basha, G. et al. Historical and projected surface temperature over India during the 20th and 21st century. *Sci. Rep.* **7**, 2987 (2017).
- Rohini, P., Rajeevan, M. & Srivastava, A. K. On the variability and increasing trends of heat waves over India. *Sci. Rep.* **6**, 26153 (2016).
- Fowler, H. J. & Archer, D. R. Conflicting signals of climatic change in the Upper Indus Basin. *J. Clim.* **19**, 4276–4293 (2006).
- Kothawale, D. R., Kumar, K. K. & Srinivasan, G. Spatial asymmetry of temperature trends over India and possible role of aerosols. *Theor. Appl. Climatol.* **110**, 263–280 (2012).
- Sethi, S. S. et al. Spatio-temporal evolution of surface urban heat island over Bhubaneswar-Cuttack twin city: a rapidly growing tropical urban complex in Eastern India. *Environ. Dev. Sustain.* <https://doi.org/10.1007/s10668-023-03254-5> (2023).
- Raj, S., Paul, S. K., Chakraborty, A. & Kuttippurath, J. Anthropogenic forcing exacerbating the urban heat islands in India. *J. Environ. Manag.* **257**, 110006 (2020).
- Dimri, A. P. Comparison of regional and seasonal changes and trends in daily surface temperature extremes over India and its subregions. *Theor. Appl. Climatol.* **136**, 265–286 (2019).
- Srivastava, A. K., Rajeevan, M. & Kshirsagar, S. R. Development of a high resolution daily gridded temperature data set (1969–2005) for the Indian region. *Atmos. Sci. Lett.* **10**, 249–254 (2009).
- Kumar, K. R., Kumar, K. K. & Pant, G. B. Diurnal asymmetry of surface temperature trends over India. *Geophys. Res. Lett.* **21**, 677–680 (1994).
- Krishnan, R. & Ramanathan, V. Evidence of surface cooling from absorbing aerosols. *Geophys. Res. Lett.* **29**, 54–1–54–4 (2002).
- Runge, J., Nowack, P., Kretschmer, M., Flaxman, S. & Sejdinovic, D. Detecting and quantifying causal associations in large nonlinear time series datasets. *Sci. Adv.* **5**, eaau4996 (2019).
- Chu, T., Glymour, C. & Ridgeway, G. Search for additive nonlinear time series causal models. *J. Mach. Learn. Res.* **9**, 967–991 (2008).
- Spirites, P. & Glymour, C. An algorithm for fast recovery of sparse causal graphs. *Soc. Sci. Comput. Rev.* **9**, 62–72 (1991).
- Pielke et al. Unresolved issues with the assessment of multidecadal global land surface temperature trends. *J. Geophys. Res. Atmos.* **112**, D24 (2007).
- Trenberth, K. E., Caron, J. M., Stepaniak, D. P. & Worley, S. Evolution of El Niño–Southern Oscillation and global atmospheric surface temperatures. *J. Geophys. Res.* **107**, AAC-5 (2002).
- Krishnan, R. et al. *Assessment of Climate Change over the Indian Region: A Report of the Ministry of Earth Sciences (MOES), Government of India* (Springer Nature, 2020).
- Dileepkumar, R., AchutaRao, K. & Arulalan, T. Human influence on sub-regional surface air temperature change over India. *Sci. Rep.* **8**, 8967 (2018).
- Hameed, S. N., Jin, D. & Thilakan, V. A model for super El Niños. *Nat. Commun.* **9**, 1–15 (2018).
- Chen, N., Thual, S. & Hu, S. *El Niño and the Southern Oscillation: Observation*. Elsevier. [https://scholar.google.co.in/scholar?hl=en&as\\_sd=0,5&cluster=14480714073943](https://scholar.google.co.in/scholar?hl=en&as_sd=0,5&cluster=14480714073943) (2019).
- Santoso, A., McPhaden, M. J. & Cai, W. The defining characteristics of ENSO extremes and the strong 2015/2016 El Niño. *Rev. Geophys.* **55**, 1079–1129 (2017).
- Jacob, M. G. et al. Impacts of the 2015–2016 El Niño on the California Current System: early assessment and comparison to past events. *Geophys. Res. Lett.* **43**, 7072–7080 (2016).

35. Bonfils, C. & Lobell, D. Empirical evidence for a recent slowdown in irrigation-induced cooling. *Proc. Natl Acad. Sci. USA* **104**, 13582–13587 (2007).
36. Puma, M. J. & Cook, B. I. Effects of irrigation on global climate during the 20th century. *J. Geophys. Res.* **115**, D16120 (2010).
37. Timmreck, C. Modeling the climatic effects of large explosive volcanic eruptions. *Wiley Interdiscip. Rev. Clim. Change* **3**, 545–564 (2012).
38. Robock, A. in *The Encyclopedia of Volcanoes* 935–942 (Academic Press, 2015).
39. Allen, S. K. et al. In *Managing the Risks of Extreme Events and Disasters to Advance Climate Change Adaptation* (eds Field, C. B., Barros, V., Stocker, T. F. & Dahe, Q.) 3–22 (Cambridge University Press, 2012).
40. Kueppers, L. M., Snyder, M. A. & Sloan, L. C. Irrigation cooling effect: regional climate forcing by land-use change. *Geophys. Res. Lett.* <https://doi.org/10.1029/2006GL028679> (2007).
41. Shi, W., Tao, F. & Liu, J. Regional temperature change over the Huang-Huai-Hai Plain of China: the roles of irrigation versus urbanization. *Int. J. Climatol.* **34**, 1181–1195 (2014).
42. Kalnay, E. & Cai, M. Erratum: Corrigendum: Impact of urbanization and land-use change on climate. *Nature* **425**, 102–102 (2003).
43. Pai, D. S., Nair, S. & Ramanathan, A. N. Long term climatology and trends of heat waves over India during the recent 50 years (1961–2010). *Mausam* **64**, 585–604 (2013).
44. Sharma, S. & Mujumdar, P. Increasing frequency and spatial extent of concurrent meteorological droughts and heatwaves in India. *Sci. Rep.* **7**, 15582 (2017).
45. Murari, K. K., Ghosh, S., Patwardhan, A., Daly, E. & Salvi, K. Intensification of future severe heat waves in India and their effect on heat stress and mortality. *Reg. Environ. Change* **15**, 569–579 (2015).
46. Rohini, P., Rajeevan, M. & Mukhopadhyay, P. Future projections of heat waves over India from CMIP5 models. *Clim. Dyn.* **53**, 975–988 (2019).
47. Kuttippurath, J. et al. Observed rainfall changes in the past century (1901–2019) over the wettest place on Earth. *Environ. Res. Lett.* **16**, 024018 (2021).
48. Al-Ghusain, L. Global warming: review on driving forces and mitigation. *Environ. Prog. Sustain. Energy* **38**, 13–21 (2019).
49. Meehl, G. A., Arblaster, J. M. & Tebaldi, C. Contributions of natural and anthropogenic forcing to changes in temperature extremes over the United States. *Geophys. Res. Lett.* <https://doi.org/10.1029/2007GL030948> (2007).
50. Utsumi, N., Seto, S., Kanae, S., Maeda, E. E. & Oki, T. Does higher surface temperature intensify extreme precipitation? *Geophys. Res. Lett.* <https://doi.org/10.1029/2011GL048426> (2011).
51. Du, M. et al. Evaluating the contribution of different environmental drivers to changes in evapotranspiration and soil moisture, a case study of the Wudaogou Experimental Station. *J. Contam. Hydrol.* **243**, 103912 (2021).
52. Chaturvedi, R. K., Joshi, J., Jayaraman, M., Bala, G. & Ravindranath, N. H. Multi-model climate change projections for India under representative concentration pathways. *Curr. Sci.* **103**, 791–802 (2012).
53. Singh, T., Mittal, R. & Shukla, M. V. Validation of INSAT-3D temperature and moisture sounding retrievals using matched radiosonde measurements. *Int. J. Remote Sens.* **38**, 3333–3355 (2017).
54. Gupta, P. et al. Validation of surface temperature derived from MERRA-2 reanalysis against IMD gridded data set over India. *Earth Space Sci.* **7**, e2019EA000910 (2020).
55. Cornes, R. C. & Jones, P. D. How well does the ERA-Interim reanalysis replicate trends in extremes of surface temperature across Europe? *J. Geophys. Res.* **118**, 10,262–10,276 (2013).
56. Rienecker, M. M. et al. MERRA: NASA's modern-era retrospective analysis for research and applications. *J. Clim.* **24**, 3624–3648 (2011).
57. Molod, A., Takacs, L., Suarez, M. & Bacmeister, J. Development of the GEOS-5 atmospheric general circulation model: evolution from MERRA to MERRA2. *Geosci. Model Dev.* **8**, 1339–1356 (2015).
58. Hersbach, H. et al. The ERA5 global reanalysis. *Q. J. R. Meteorol. Soc.* **146**, 1999–2049 (2020).
59. Kalnay, E. et al. The NCEP/NCAR 40-year reanalysis project. *Bull. Am. Meteorol. Soc.* **77**, 437–471 (1996).
60. Kistler, R. et al. The NCEP–NCAR 50-year reanalysis: monthly means CD-ROM and documentation. *Bull. Am. Meteorol. Soc.* **82**, 247–267 (2001).
61. Eyring, V. et al. Overview of the Coupled Model Intercomparison Project Phase 6 (CMIP6) experimental design and organization. *Geosci. Model Dev.* **9**, 1937–1958 (2016).
62. Runge, J. Discovering contemporaneous and lagged causal relations in auto-correlated nonlinear time series datasets. In *Conference on Uncertainty in Artificial Intelligence* 1388–1397 (PMLR, 2020).
63. Kumar, P., Kuttippurath, J. & Mitra, A. Causal discovery of drivers of surface ozone variability in Antarctica using a deep learning algorithm. *Environ. Sci. Process. Impacts* **24**, 447–459 (2022).
64. Chambers, D. P., Tapley, B. D. & Stewart, R. H. Anomalous warming in the Indian Ocean coincident with El Niño. *J. Geophys. Res.* **104**, 3035–3047 (1999).
65. Annamalai, H., Hamilton, K. & Sperber, K. R. The south Asian summer monsoon and its relationship with ENSO in the IPCC AR4 simulations. *J. Clim.* **20**, 1071–1092 (2007).

## ACKNOWLEDGEMENTS

We thank the Head, CORAL and the Director, Indian Institute of Technology Kharagpur (IITKG) for providing the facility for this study. R.K. acknowledges research fellowship from the Ministry of Education (MoES). We also thank the ISRO RESPOND programme through Space Application Centre (SAC) Ahmedabad and KCSTC of IIT Kharagpur for supporting the study. G.S.G. acknowledges the INSPIRE fellowship provided by the Department of Science and Technology, Ministry of Science and Technology for funding his Doctoral fellowship at IIT KGP. This research received no funding.

## AUTHOR CONTRIBUTIONS

R.K.: methodology, software, formal analysis, investigation, data curation, visualisation, writing—original draft. J.K.: conceptualisation, methodology, formal analysis, investigation, visualisation, resources, writing—original draft, writing—review and editing, supervision. P.K., G.S.G., H.V.: data curation, visualisation, investigation, writing—review and editing.

## COMPETING INTERESTS

The authors declare no competing interests.

## ADDITIONAL INFORMATION

**Supplementary information** The online version contains supplementary material available at <https://doi.org/10.1038/s41612-023-00494-0>.

**Correspondence** and requests for materials should be addressed to Jayanarayanan Kuttippurath.

**Reprints and permission information** is available at <http://www.nature.com/reprints>

**Publisher's note** Springer Nature remains neutral with regard to jurisdictional claims in published maps and institutional affiliations.



**Open Access** This article is licensed under a Creative Commons Attribution 4.0 International License, which permits use, sharing, adaptation, distribution and reproduction in any medium or format, as long as you give appropriate credit to the original author(s) and the source, provide a link to the Creative Commons license, and indicate if changes were made. The images or other third party material in this article are included in the article's Creative Commons license, unless indicated otherwise in a credit line to the material. If material is not included in the article's Creative Commons license and your intended use is not permitted by statutory regulation or exceeds the permitted use, you will need to obtain permission directly from the copyright holder. To view a copy of this license, visit <http://creativecommons.org/licenses/by/4.0/>.

© The Author(s) 2023